Self-organized anteroposterior regionalization of early midbrain and hindbrain using micropatterned human embryonic stem cells

Tianfa Xie[1], Lauren E. Brown[2], ChangHui Pak[3] and Yubing Sun[1,2]*

[1]Department of Mechanical and Industrial Engineering, University of Massachusetts, Amherst, Massachusetts 01003, USA

[2]Department of Biomedical Engineering, University of Massachusetts, Amherst, Massachusetts 01003, USA

[3]Department of Biochemistry and Molecular Biology, University of Massachusetts, Amherst, Massachusetts 01003, USA

*****Correspondence: ybsun@umass.edu (Yubing Sun)

KEYWORDS

Human embryonic stem cells, anteroposterior, midbrain, hindbrain, micropatterning

SUMMARY

To develop into the central nervous system, neuroepithelial cells must first form a neural tube consisting of a series of patterned neural progenitor cells along the anterior-posterior (AP) axis. Based on studies using model organisms, it has been revealed that AP spatial regionalization is dominated by gradients of morphogens that regulate retinoic acid (RA), sonic hedgehog (SHH), bone morphogenetic proteins (BMPs), and Wingless/int1 (WNT) signaling pathways. Recently, human pluripotent stem cells (hPSCs) were successfully induced into a patterned neural tissue with differential AP gene expression levels by a gradient of WNT activity controlled by a microfluidic device. However, the midbrain and hindbrain boundaries were not as sharp as observed in vivo, likely due to the lack of additional important morphogenic factors, such as RA and SHH. Here, we induced micropatterned hPSCs into AP patterned neural tissue by activating not only WNT but also RA and SHH signals under fully defined culture conditions. We found that hPSCs self-organized into spatially patterned midbrain ($FOXG1^{-}OTX2^{+}$) and hindbrain ($HOXB4^{+}$) progenitors with a sharp boundary after 6 days of induction. Following the initial induction, the cells with midbrain identities near the pattern boundary folded inwardly to form a 3D structure, maintaining a distinct boundary between $OTX2^{+}$ and $HOXB4^{+}$ zones. To investigate the mechanism of cell fates patterning, we found that the reaction-diffusion of BMP/Noggin played a role in AP regionalization, while differential mechanical stress and cell sorting were unlikely to be involved. Then, we validated our model by investigating the effects of exposure to two known teratogens including valproic acid and isotretinoin. Drug treatment results successfully predicted that valproic acid inhibited the development of both midbrain and hindbrain development while isotretinoin disrupts the normal AP patterning of the midbrain and

hindbrain. In conclusion, by integrating engineering approaches and chemically defined culture conditions, we have developed an *in vitro* AP patterned model of early human midbrain and hindbrain development, and we have revealed its potential to be employed as a high throughput drug discovery system.

INTRODUCTION

To develop into the central nervous system, the neural tube first must be formed with a pattern consisting of organized neural progenitors along the anterior-posterior (AP) axis[1,2]. A series of three vesicles then emerge at the anterior end of the neural tube[3]. These vesicles are known as the forebrain (prosencephalon, which soon divides into diencephalon and telencephalon), the midbrain (mesencephalon, which grows into the adult brainstem[4]), and the hindbrain (rhombencephalon, which subsequently splits into the rostral metencephalon and caudal myelencephalon)[1]. The rostral metencephalon then develops into pons and cerebellum[4] while the caudal myelencephalon grows into medulla oblongata[5]. Secondary organizing centers such as the midbrain-hindbrain boundary, also termed as the isthmus, which functions as an organizer for the midbrain and hindbrain, form subsequently to impose local signaling gradients to sequentially pattern the neural tube into subregions[2,4,6,7].

Based on studies[8-10] using model organisms such as *Xenopus*, chicks, and zebrafish, it is understood that AP patterning is regulated by several diffusible factors including retinoic acid (RA), sonic hedgehog (SHH), fibroblast growth factors (FGFs), bone morphogenetic proteins (BMPs), and Wnts[11]. These factors are secreted from surrounding tissues such as the somites, notochord, and dorsal ectoderm to form gradients of signals[5,6,12].

Recently, *in vitro* development models using human pluripotent stem cells (hPSCs) have provided opportunities for investigating how neural tube is developed and patterned in human[13-15]. For instance, dorsal-ventral patterning models have been successfully generated via guided self-organization of neural cysts[16,17], by microfluidic diffusion-based gradient generators[18], or by

organoid fusion techniques[19-21]. In addition, by activating WNT or RA signaling, forebrain, midbrain, or rostral hindbrain fates could be obtained in a dose-dependent manner from hPSCs using a defined protocol[16,22-24]. However, none of these generated tissues consist of patterned midbrain and hindbrain simultaneously. Recently, using a microfluidic device to generate a single gradient of WNT signaling, a patterned neural tissue was generated with AP gene expression patterns observed in mouse embryos[25]. However, the boundaries between midbrain and hindbrain are not as sharp as observed *in vivo*, which is likely due to the lack of additional morphogenic factors involved in neural tube patterning, such as RA[7]. To our knowledge, the AP neural patterning with an embryo-like sharp boundary between the midbrain and hindbrain has not been generated *in vitro*.

Here, we have developed an *in vitro* model for AP neural patterning using hPSCs by regulating RA, BMP, SHH, and WNT signals. We found that the reaction-diffusion of BMP/Noggin played a role in AP regionalization of $OTX2^+$ midbrain and $HOXB4^+$ hindbrain tissues. We further demonstrated that the model could predict the effects of different teratogens on the midbrain and hindbrain development. In the future, our platform can be used to investigate the mechanisms of human AP neural regionalization and border formation in neural development at the molecular level.

MATERIALS AND METHODS

Cell culture: Both SOX10 :: EGFP bacterial artificial chromosome hES cell reporter line (H9; WA09, WiCell; NIH registration number: 0062; female; generated by Dr. Lorenz Studer's lab[26]) and control human induced pluripotent stem (hiPS) cell line (male; generated from human

primary T-cells using episomal reprogramming method) were cultured in Essential 8 growth medium on hES cell-qualified Geltrex (Thermo Fisher Scientific). Karyotyping and mycoplasma testing were performed routinely to ensure genomic integrity. After treatment with EDTA dissociation buffer (5 min at 37 °C), the cells were collected using a cell scraper (BD Biosciences), centrifuged (200 g for 5 min), and re-dispersed in Essential 8 growth medium supplemented with ROCKi (Y27632, 10 μM; Cayman Chemical) before cell seeding. The induction media are comprised of Essential 6 basal media, TGF-β inhibitor SB431542 (SB, Cayman Chemical; 10 μM), WNT agonist CHIR99021 (CHIR, Cayman Chemical; 60 nM), all-trans retinoic acid (RA, Cayman Chemical; 500 nM), smoothened agonist (SAG, Cayman Chemical; 1 μM), and BMP4 recombinant protein (Gibco; 5 ng/mL). The media was half-changed every day during the differentiation process. All cells were cultured at 37 °C and 5% CO_2.

Microcontact printing: Soft lithography was used to generate micropatterned polydimethylsiloxane (PDMS) stamps from negative SU8 molds that were fabricated using photolithography. These PDMS stamps were used to generate micropatterned cell colonies using microcontact printing, as described previously[27]. Briefly, to generate micropatterned cell colonies on flat PDMS surfaces, round glass coverslips (diameter = 25 mm, Fisher Scientific) were spin-coated (Spin Coater; Laurell Technologies) with a thin layer of PDMS prepolymer comprising of PDMS base monomer and curing agent (10:1 *w*/*w*; Sylgard 184, Dow-Corning). PDMS coating layer was then thermally cured at 110 °C for at least 24 h. In parallel, PDMS stamps were incubated with a vitronectin solution (20 μg ml^{-1}, in deionized water) for 1 h at room temperature before being blown dry with a stream of nitrogen. Excess vitronectin was then

washed away by distilled water and the stamps were dried under nitrogen. Vitronectin-coated PDMS stamps were then placed on top of ultraviolet ozone-treated PDMS (7 min, UV-ozone cleaner; Jetlight) on coverslips with a conformal contact. The stamps were pressed gently to facilitate the transfer of vitronectin to PDMS-coated coverslips. After removing stamps, coverslips were disinfected by submerging in 70% ethanol. Protein adsorption to PDMS surfaces without printed vitronectin was prevented by incubating coverslips in 0.2% Pluronic F127 solution (P2443-250G, Sigma) for 30 min at room temperature. Coverslips were rinsed with PBS before being placed into tissue culture plates for cell seeding. For micropatterned cell colonies, PDMS stamps containing circular patterns with diameters of 600 μm were used if not specifically indicated.

Immunocytochemistry: 4% paraformaldehyde (Electron Microscopy Sciences) was used for cell fixation before permeabilization with 0.1% Triton X-100 (Fisher Scientific) at 4 °C on an orbital shaker (20 rpm) for 24 hours. Then cells were blocked in 4% donkey serum with 0.1% Triton X-100 on an orbital shaker (20 rpm) for 24 hours at 4 °C. Then samples were incubated with primary antibodies (listed in the appendices) diluted in antibody dilution buffer (4% DS, 0.1% Triton-X 100 in sterile PBS) at 4 °C for 48 hours. Finally, samples were incubated with secondary antibodies at 4 °C for 24 hours. Samples were counterstained with 4,6-diamidino-2-phenylindole (DAPI; Invitrogen) to visualize the cell nucleus. The primary antibodies used in this study include HoxB4 (rat, DSHB, I12, 1:20), OTX2 (goat, R&D Systems, 1:100), and PAX6 antibodies (mouse, Abcam, Ab78545, 1:100). The I12 anti-Hoxb4 monoclonal antibody193, developed by Gould, A. / Krumlauf, R in MRC National Institute for Medical Research, was obtained from the Developmental Studies Hybridoma Bank, created by the NICHD of the NIH

and maintained at The University of Iowa, Department of Biology, Iowa City, IA 52242. For immunolabelling, donkey-anti goat IgG-Alexa Fluor 647 (1:1000, Life Technologies), donkey-anti rat IgG-Alexa Fluor 488 (1:1000, Life Technologies), donkey-anti rabbit IgG-Alexa Fluor 555 (1:1000, Life Technologies) secondary antibodies were used.

Image acquisition and analysis: Confocal images were collected with NIS-Elements AR software using Nikon A1 Resonant scanning confocal inverted microscope. Alexa Fluor 488 was excited with a 488 nm laser line. Alexa Fluor 555 was excited with a 561 nm laser line. Alexa Fluor 647 was excited with a 640 nm laser line. 10× objective was used. Data analysis was performed using the NIS-Elements AR analysis software. All other phase contrast and fluorescence images of micropatterned cell colonies were recorded using an inverted epifluorescence microscope (Leica DMi8; Leica Microsystems) equipped with a monochrome charge-coupled device (CCD) camera. Images were first cropped using a custom-developed MATLAB program (MathWorks; https://www.mathworks.com/) to a uniform square with pattern centroids aligned.

Cell colonies with a non-radially symmetric cell density pattern or with disorganized cellular structures were excluded from data analysis. The fluorescence intensity of each pixel in cropped images was normalized by the maximum intensity identified in each image. These normalized images were stacked together to obtain average intensity maps. To plot average intensity as a function of distance from colony centroid, average intensity maps for circular cell colonies were divided into 100 concentric zones with equal widths. The average pixel intensity in each concentric zone was calculated and plotted against the mean distance of the concentric zone from

the colony centroid. From average intensity plots of cell lineage markers, values of the full width at half maximum (FWHM) were determined as the difference between the two radial positions at which the average fluorescence intensity of individual markers is equal to half of its maximum value.

Pharmaceutical inhibitions assays: Blebbistatin (10 µM, Cayman Chemical), Y27632 (10 µM, Cayman Chemical), IWP2 (3 µM, Cayman Chemical), GANT61 (10 µM, Cayman Chemical), LDN193189 (500 nM, Cayman Chemical), and AGN193109 (100 nM, MedChemExpress) were dissolved in dimethyl sulfoxide (DMSO, Sigma-Alrich). Cells were treated with these drugs for 48 and/or 72 hours at 37 °C.

Cell Proliferation Assay (MTS): To determine the cytotoxicity of drugs, 10,000 hESCs/well were seeded into each well of 96-well plates with E8 supplemented with Y27632 and cultured overnight. The medium supplemented with Y27632 was changed to E8 and then the cells were treated with the selected drugs with 8 serial concentrations with 4 (for isotretinoin) or 5 (for valproic acid and penicillin G) times dilution factor along with solvent for 48 hours. The medium supplemented with drugs was changed daily. The cell proliferation assay was conducted with CellTiter 96® AQ$_{ueous}$ One Solution Cell Proliferation Assay (MTS) reagent (Promega, Cat.No. G3582) following the instruction. The absorbance was measured using a plate reader (Cytation 3 microplate reader, BioTek Instruments Inc, Winooski, VT, USA). The corrected absorbance at 490 nm was plotted versus the concentrations of the drugs. The IC_{25} values were determined manually using GraphPad Prism 7.

Drug-screening assay: Valproic acid (Cat. No. P4543, Sigma-Aldrich) and penicillin G (Cat. No. 13752-1G-F, Sigma-Aldrich) were dissolved in Milli-Q water. Isotretinoin (Cat. No. 21648, Cayman Chemical) was dissolved in DMSO. The cells were induced with Essential 6 medium supplemented with these drugs as well as other factors starting from day 2 until day 6 and/or 7. The medium was half-changed daily.

Statistical analysis: Student's t-test was used when there were two groups. One-way ANOVA and post-hoc Tukey's test were used for three or more groups. Mann–Whitney test was used for data that was found not normally distributed. Data are represented as mean ± s.e.m. The *n* values are determined using G*Power, using the standard deviation and effect size from pilot experiments, with a type I error rate $\alpha = 0.05$ and power of 80%. In all cases, the actual *n* values are significantly larger than the desired *n* value. All the experiments were repeated at least 3 times independently (biological replicates), and in each experiment, at least two technical replicates (replicates within each experiment) were used. Samples were randomly allocated into experimental groups in the drug treatment experiments, while masking was not used during group allocation, data collection, and/or data analysis.

RESULTS

Generation of AP patterned human neural tissues

We first investigated whether activating RA, SHH, BMP, and WNT signaling pathways could induce anterior and posterior neuroepithelial cells simultaneously from hPSCs monolayers. After two days of neural induction with fully defined Essential 6 (E6) media supplemented with a TGF-β inhibitor SB431542 (SB, 10 μM), we induced H9 human embryonic stem cells (ESCs)

with added neural tube morphogenic factors including RA (500 nM), BMP4 recombinant protein (5 ng/ml), SHH pathway agonist (SAG, 1 μM), and WNT pathway agonist CHIR99021 (CHIR, 60 nM) for two or three more days (**Supplementary Figure 1**). By continuously inhibiting TGF-β and activating RA, SHH, BMP, and WNT signals, we found that H9 human ESCs could successfully differentiate into both anterior and posterior neural tissues as verified by co-staining HOXB4 as a hindbrain marker and OTX2 as a marker for forebrain and midbrain progenitors (**Supplementary Figure 2**). However, both cell types were randomly distributed and mixed without distinct spatial organization (**Supplementary Figure 2**).

As our previous work demonstrated that geometrically confined hPSCs could self-organize into patterned neuroectoderm[28,29], we next studied whether geometrical confinement could facilitate the formation of spatial AP patterning. After plating human ESCs in circular micropatterned substrate (diameter, 600 μm) and inducing cell differentiation using the same protocol (**Supplementary Figure 1**), we found that AP patterned human neural tissues were successfully generated. On day 6, human ESCs self-organized into structures with two distinct zones (**Figure 1A,** top panel). The cells located at the center of the micropattern were $OTX2^+$, indicating a forebrain/midbrain cell fate[4]. Hindbrain marker $HOXB4^+$ cells are predominately located at the boundary of the micropattern. A distinct boundary could be observed between the OTX2 and HOXB4 layers, as seen in the epifluorescence images, heatmap, and intensity plots (**Figure 1A, 1B,** and **1C**). We observed similar AP patterning of OTX2 and HOXB4 using an independent human-induced pluripotent stem cell (iPS) line (**Supplementary Figure 3**).

Surprisingly, a drastic change in cell positioning was observed after extending the tissue culture. We found that on day 7, hindbrain marker HOXB4^{+} cells were located within a ring region in the middle of the micropattern (**Figure 1A)** and that the boundary cells expressed OTX2. To elucidate the tissue structure, we first performed z-stack confocal microscopy to visualize the cross-section profile of the micropatterned human neural tissue. As revealed in the cross-sectional view, HOXB4^{+} cells were stacking on top of the bottom layer of OTX2^{+} cells, suggesting that the HOXB4^{+} cells that were located on the boundary on day 6 subsequently folded inwardly to the center of the micropattern to form the ring structure (**Figure 1D** and **Figure 1E)**. We next performed time-lapse live-cell imaging from day 6 to day 7 to capture the dynamics of the process (**Supplementary Figure 4**). This morphological change was then confirmed to be caused by cell folding (**Supplementary Figure 4** and **Supplementary Movie**). The bright-field images and the movie showed that the front cells (presumably HOXB4^{+} cells) were moving inwardly while maintaining a distinguishable boundary with the follower cells (presumably OTX2^{+} cells), which is consistent with our immunostaining results.

Next, to further characterize the cell fates, we performed immunostaining for other neural markers including PAX6 (as a neuroepithelial marker), N-cadherin (as a neuroepithelial marker), FOXG1 (as a forebrain marker[21,30]), and GBX2 (as an anterior hindbrain marker[2]) (**Supplementary Figure 5**). We performed z-stack confocal microscopy and found that almost all the cells in both layers are PAX6^{+} and N-cadherin^{+} on day 7, further confirming the neuroepithelial identity of the cells[23,28]. In addition, the immunostaining results showed that the FOXG1 signal was not detectable across the micropattern and that very few GBX2 expressing

cells colocalized with OTX2$^+$ region, suggesting OTX2$^+$ midbrain and GBX2$^+$ anterior hindbrain were not completely separated at this early stage.

The mechanism of AP patterning of OTX2 and HOXB4 regions

To understand how the OTX2/HOXB4 pattern was formed, we studied three possible mechanisms, which are cell sorting, differential mechanical stress, and reaction-diffusion (RD) derived biochemical gradient. Firstly, differential tissue interfacial tension has been proposed to explain cell sorting and compartmentalization[31,32]. To test whether the AP patterning of OTX2 and HOXB4 was formed via cell sorting, we fixed the cells and performed immunostaining at two earlier time points including 136 h and 140 h (**Figure 2A**), and compared with the results at 144 h (i.e., day 6). We found that at 136 h, OTX2$^+$ cells had emerged in the pattern center while the HOXB4 signals were very weak (**Figure 2A**). At 140 h, the HOXB4 signals had become detectable at the boundary of the micropatterns (**Figure 2A**). As the mixture of these two types of cells at an earlier stage was not found, it is unlikely that cell sorting is involved in the formation of two separated layers of midbrain and hindbrain tissues.

We and others have reported that differential mechanical tension controls cell fates determination such as neural plate and neural plate border cells[28], and mesoderm specification[33]. Thus, we asked whether differential mechanical tension of the boundary and center cells contributed to the midbrain/hindbrain cell fates patterning. We treated the cells with myosin inhibitor (Blebbistatin, 10 μM) or ROCK inhibitor (Y27632, 10 μM), two small molecules widely used to inhibit cellular actomyosin contractility. After treatment with these two drugs from day 4 to day 6, we found that the AP patterning of OTX2 and HOXB4 remained the same as the vehicle control

(**Figure 2B-D**). In addition, we performed immunostaining to investigate whether HOXB4 overlapped with cell nuclei localized Yes-associated protein (YAP), which is a Hippo signaling pathway effector and has been identified as a key mechanotransducer that senses mechanical stimuli. We found that most HOXB4$^+$ cells did not show significant overlaps with nuclear YAP$^+$ cells (**Supplementary Figure 6**). Together, these results suggested that differential mechanical tension was not required for midbrain/hindbrain patterning.

Our prior work showed that reaction-diffusion of multiple morphogens may synergistically regulate spatial cell fate patterning in micropatterned hPSCs[29]. To test this possibility, we first investigated the effects of pattern sizes on the regionalization of cell fates since reaction-diffusion patterns changes with tissue size. The immunostaining images showed that the midbrain/hindbrain cell patterning remained the same for smaller pattern sizes such as 200 or 400 μm. Interestingly, some colonies with diameters of 800 or 1000 μm showed a periodic regionalization of HOXB4$^+$ cells with OTX2$^+$ cells flanked by two layers of HOXB4$^+$ cells at the boundary and the center of the pattern (**Figure 3A**). This result suggested that HOXB4 cell fate was determined by one or more morphogens with their activities changing periodically across the pattern, which is a characteristic of reaction-diffusion.

We next sought to elucidate the functional roles of SHH, RA, WNT, and BMP in the midbrain/hindbrain patterning by treating the cells with inhibitors of these signaling pathways from day 4 to day 6. We found that treating cells with GANT61, a sonic hedgehog pathway inhibitor, did not change the OTX2 and HOXB4 localizations (**Supplementary Figure 7**). In contrast, cells treated with AGN193109 (a RA signal inhibitor), IWP2 (a WNT inhibitor), or

LDN193189 (a BMP inhibitor) displayed weaker HOXB4 signal and disrupted patterning of HOXB4 and OTX2, suggesting the involvement of RA, WNT and BMP4, but not SHH signaling. To clarify whether their contributions are permissive or instructive, we changed the concentrations of RA, CHIR, and BMP4 added to the media, respectively. We found that lowering RA concentration to 0.1 μM led to weaker HOXB4 signals without changing the relative localization of OTX2 and HOXB4 expressions (**Supplementary Figure 8**). Similarly, lowering CHIR concentration to 30 nM or increasing it to 600 nM did not significantly change the midbrain/hindbrain patterning. Notably, the cells induced with high CHIR concentration (600 nM) displayed similar patterns that were observed in cells induced with intermediate CHIR (60 nM) on day 7 (**Supplementary Figure 9** and **Figure 1A**), which can be explained by the effects of WNT activation on cell proliferation. However, when cells were induced with a high concentration of BMP4 (10 ng/ml), the area covered by $OTX2^+$ cells became significantly smaller and the peak of HOXB4 signals shifted dramatically inwardly to the center of the micropattern (**Figure 3B, 3C, and 3D**). Reducing BMP4 concentration to 1 ng/ml led to the expansion of the $OTX2^+$ zones. Together, our data suggest that RA and WNT are permissive signals that are required for the caudalization, while the BMP4 signal instructs the midbrain/hindbrain patterning.

Drug-induced developmental defects in early midbrain and hindbrain

Several teratogens have been identified that disrupt the midbrain/hindbrain development[34-37]. For example, valproic acid (VPA) exposure during embryo development causes neural tube defects and other types of malformations such as smaller midbrain size and an increase in the midline gap of the hindbrain[38,39]. It also decreases the proliferation of neuronal progenitor cells in early

development[38]. In addition, recent clinical studies show that exposure to isotretinoin during pregnancy was linked to midbrain/hindbrain development malformations featured as disproportionately long midbrain and dysplasia of the quadrigeminal plate and vermis and disrupted AP axis patterning[37,40-43].

To further validate our model, we investigated the developmental toxicity caused by VPA and isotretinoin on the midbrain/hindbrain patterning. We induced human ESCs into midbrain and hindbrain cells in the presence of low dosages of VPA and isotretinoin. Penicillin G was used as a non-teratogenic control since it has been shown that it does not disrupt neural tube development at its peak plasma concentration[44-46]. First, we performed cell proliferation assay to measure cell viability under treatment with different concentrations of these three tested drugs (**Supplementary Figure 10**). Based on the cell viability curves, we determined the 25% inhibition concentrations (IC_{25}) for these three drugs to find their range of non-cytotoxic concentration levels (**Supplementary Table 2**). Then, we selected three concentrations designated as the low, medium, and high concentrations based on the IC_{25} levels and their peak plasma concentrations (**Supplementary Table 2** and **Supplementary Table 3**). To mimic exposure to penicillin G, VPA, or isotretinoin during embryonic development, we treated the human ESCs with these three drugs as well as DMSO as a control group starting from day 2 and performed the same differentiation protocol for midbrain and hindbrain differentiation (**Supplementary Figure 1**).

As expected, the results showed that all the low (40 µg/ml), medium (200 µg/ml), and high (1000 µg/ml) dosages of penicillin G treated groups did not alter the midbrain/hindbrain lineage

specification and spatial patterning (**Supplementary Figure 11, Figure 4**, and **Supplementary Figure 12**). In contrast, after treatment with the medium dosage of VPA (0.12 mM), the area covered by OTX2$^+$ cells decreased significantly compared to either DMSO control or penicillin G treated group on day 6 while the HOXB4 signal was detectable on day 7 but not on day 6 (**Figure 4A** and **Figure 4G**), suggesting that VPA not only inhibited the development of OTX2$^+$ midbrain progenitors but also delayed HOXB4$^+$ hindbrain cell fate acquisition. Similar results were shown in the low (0.06 mM) and high (0.25 mM) dosages of VPA-treated groups (**Supplementary Figure 11** and **Supplementary Figure 12**). Interestingly, medium concentration (1.63 µM) of isotretinoin-treated colonies showed a randomly mixed population of OTX2$^+$ and HOXB4$^+$ cells without a boundary (**Figure 4A**), indicating that isotretinoin disrupted the normal AP patterning of OTX2 and HOXB4. In addition, the results showed that the percentage of OTX2$^+$ covered area decreased significantly, compared with the DMSO control or penicillin G treated group (**Figure 4A and Figure 4G**). The low (1.08 µM) and high (3.25 µM) dosages of isotretinoin treated group displayed similar results (**Supplementary Figure 11**, and **Supplementary Figure 12)**. These observations are consistent with the effects of VPA and isotretinoin on midbrain/hindbrain development *in vivo*, suggesting that our model can distinguish teratogens with different mechanisms.

DISCUSSION AND CONCLUSION

In this work, we demonstrate that micropatterned hPSCs can self-organize into distinct zones with midbrain and hindbrain cell fates, when RA, BMP4, and WNT signals are activated. Studies using mouse embryos reveal that the formation of midbrain-hindbrain boundary is mainly mediated by the mutually exclusive GBX2 and OTX2 signals. Interestingly, while in mice the

GBX2$^+$ and OTX2$^+$ domains are separated initially before the gap closes[47], our findings suggest that in humans, GBX2$^+$ and OTX2$^+$ domains are overlapped (**Supplementary Figure 5**) before they eventually become mutually exclusive. This discrepancy between human and mouse development requires further validation from *in vivo* experiments.

Our mechanistic studies show that BMP/Noggin reaction-diffusion dictates the midbrain/hindbrain patterning. While the concentration of BMP4 but not CHIR regulated the sizes of OTX2$^+$ zones and location of HOXB4$^+$ zones, we did not consider the possibility of signaling crosstalks. For instance, it has been revealed that BMP4 could trigger the activation of WNT signaling pathway during gastrulation[48,49]. Further studies will be needed to address the detailed mechanism of how BMP activity regulates the HOXB4 or OTX2 cell fate determination and whether it is via the WNT and/or RA pathway.

VPA has been known to be teratogenic since the early 1980s[34] and exposure to VPA during human embryo development has been found tightly linked to neural tube defects[35] and malformations in the midbrain and hindbrain[38,39,50,51], as well as neurological disorders such as severe cognitive defects, autism spectrum disorder, and schizophrenia[52,53]. Recently, cytoskeletal protein MARCKSL1, which is an actin-stabilizing protein essential for dendrite morphogenesis and synapse maturation, has been identified to mediate VPA-induced morphological defects in developing neurons[54]. In addition, it has been found with a human cortical organoid-on-a-chip model that the transcriptional regulation of genes such as KLHL1, LHX9, and MGARP could be a mechanism for prenatal VPA exposure induced postnatal brain disorders such as autism[55]. Isotretinoin exposure during early pregnancy has been known to be associated with an increased

risk for infant brain malformation[40,42,43,56] such as hypoplasia of the cerebellar vermis, microencephaly, vermis hypoplasia, dysplastic quadrigeminal plate, disproportionate size between midbrain and pons[40,57,58]. Known as a retinoic acid analog, isotretinoin (13-cis retinoic acid) likely acts on the retinoic acid signaling pathway to regulate the expression of Hox genes development and thus the spatial patterning of the midbrain and hindbrain. However, the detailed mechanism of these two drugs causing developmental defects, especially in the human genetic background, remains to be investigated. Using our model, it is promising to investigate how VPA and isotretinoin cause the defects in human early midbrain and hindbrain development and patterning.

It is notable that our *in vitro* midbrain/hindbrain model so far can mimic only the early-stage development of the human brain since the total duration of organized cell culture is limited due to the geometrical confinement. Extended culture of cells beyond 7 days leads to disorganized cell aggregates or clusters. Despite these disadvantages, our model is complementary to current animal models and traditional 2D cell culture systems. Compared to animal models, our system utilizes pluripotent stem cells with human genetic background and features simpler experimental procedures and a shorter time frame (~ 2 weeks). Compared to 2D cell culture, the unique phenotypes including completely separated midbrain/hindbrain zones and tissue folding can be used to quantify developmental defects. When combined with genetic engineering and automated image processing tools, we envision that our system has the potential to evolve into a high-throughput screening platform for teratogens and toxicology testing.

In conclusion, we have developed an *in vitro* model for AP patterned midbrain/hindbrain tissues using hPSCs by modulating RA, BMP, SHH, and WNT signals. The regionalization of midbrain and hindbrain cells is mainly mediated by the reaction-diffusion of BMP/Noggin. In addition, we show that our model can be used to predict the distinct effects of different teratogens on midbrain/hindbrain development. This model will provide an excellent experimental platform to investigate the mechanism of human brain development and patterning.

ACKNOWLEDGMENT

This work is supported in part by the National Science Foundation (CMMI 1846866 to Y.S.), and the National Institute of Diabetes and Digestive and Kidney Diseases (R01DK129990). The Conte Nanotechnology Cleanroom Lab is acknowledged for support in microfabrication. We also acknowledge the Light Microscopy Facility where confocal microscopy data were collected.

AUTHOR CONTRIBUTIONS

T.X. and Y.S. designed the experiments, T.X. performed all experiments, T.X. and L.B analyzed data, C. P. generated the human induced pluripotent stem cell line. All authors wrote and approved the manuscript.

DECLARATION OF INTERESTS

The authors declare no competing interests.

FIGURES

Figure 1

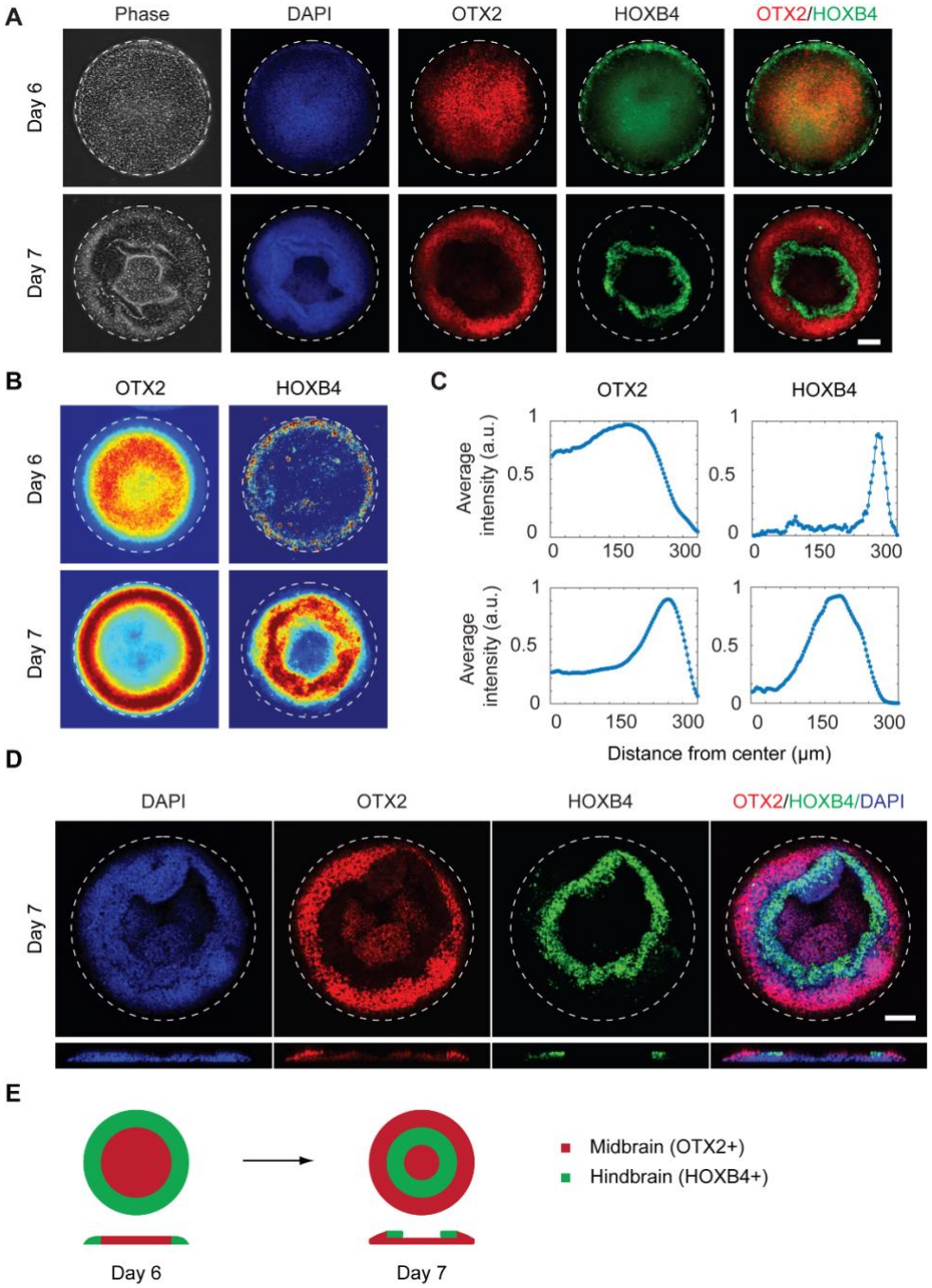

Figure 1. hPSCs self-organized into anteroposterior patterning of midbrain and hindbrain on micropatterned substrates. (A). Representative phase-contrast and immunostaining

fluorescence images showing the spatially patterned expression of anterior (OTX2) and posterior (HOXB4) neural markers on day 6 and day 7. The OTX2 and HOXB4 merged image was shown. Cell nuclei were counterstained with DAPI. (B). Colorimetric maps showing the average fluorescent intensity of OTX2 and HOXB4 staining. The intensity of each pixel of the images was normalized to the maximum value for each image. $n > 15$. (C). Plots showing the quantitative average intensity in relation to the distance to the center of the pattern. (D). Representative confocal images and the reconstructed side view showing the three-dimensional architecture and the spatial expression of OTX2+ and HOXB4+ cells on day 7. Cell nuclei were counterstained with DAPI. (E). A schematic showing the self-organized anteroposterior patterning generated from human ESCs as well as the folding process and 3D structural change from day 6 to day 7. In these experiments, H9 human ESCs were differentiated with the induction protocol. Scale bar, 100 μm.

Figure 2

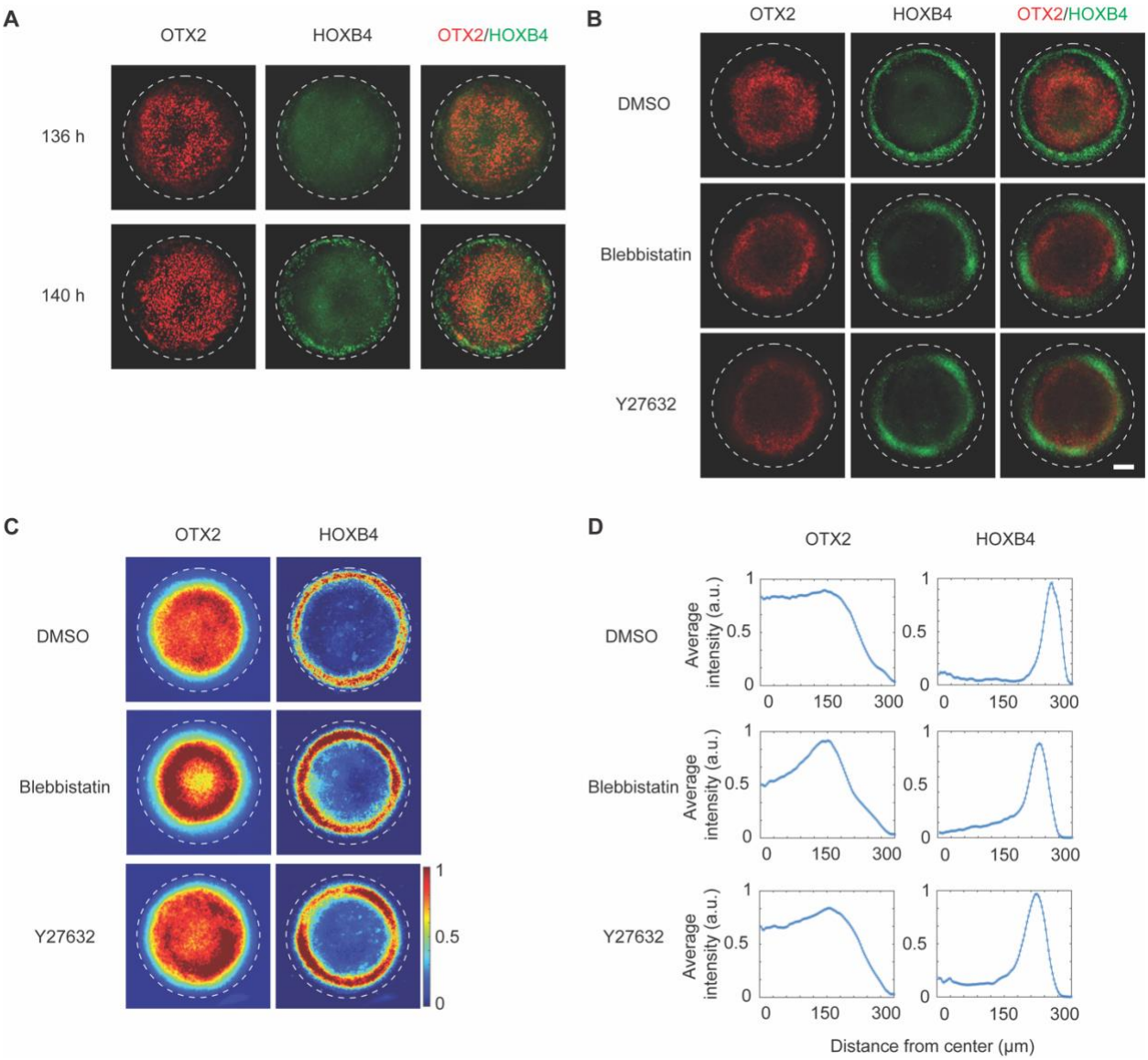

Figure 2. Cell sorting and differential mechanical stress are not the mechanisms that drive the formation of HOXB4 and OTX2 patterning. (A). Representative immunostaining fluorescence images showing the spatial expression of neural markers: OTX2 and HOXB4 at 136 hours and 140 hours. The OTX2 and HOXB4 merged image was shown. (B). Representative immunostaining fluorescence images showing the spatial expression of OTX2 and HOXB4 for

the DMSO control group, Blebbistatin (a myosin inhibitor, 10 μM) treated group, and Y27632 (a ROCK inhibitor, 10 μM) treated group. The OTX2 and HOXB4 merged image was shown. (C). Colorimetric maps showing the average fluorescent intensity of OTX2 and HOXB4 staining. The intensity of each pixel of the images was normalized to the maximum value for each image. n > 15. (D). Plots showing the quantitative average intensity of OTX2 and HOXB4 in relation to the distance to the center of the pattern. Scale bar, 100 μm.

Figure 3

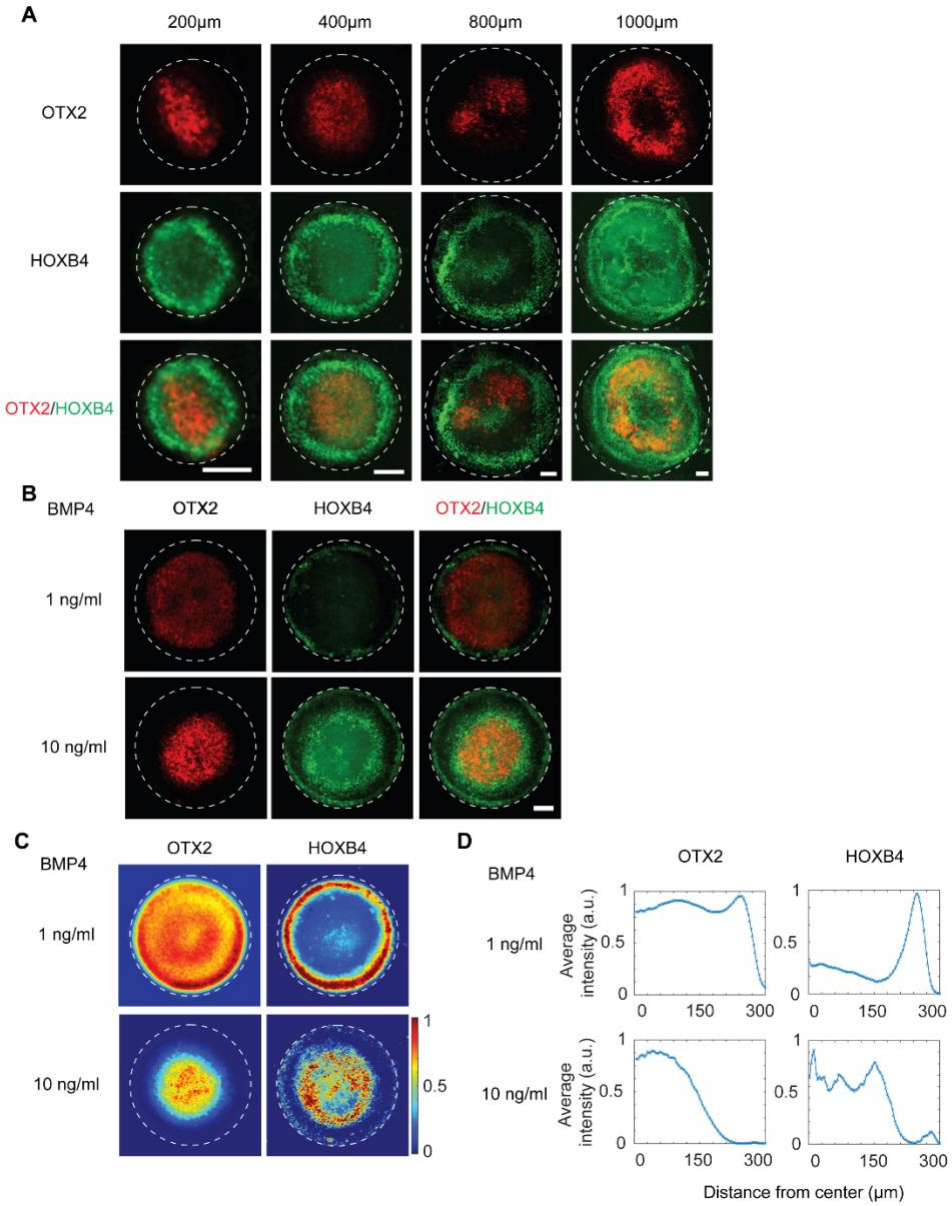

Figure 3. Reaction-diffusion of BMP/Noggin regulates the anteroposterior patterning of OTX2 and HOXB4. (A). Representative immunostaining fluorescence images showing the spatial expression of OTX2 and HOXB4 across micropatterns with diameters of 200 μm, 400 μm, 800 μm, or 1000 μm. (B). Representative immunostaining fluorescence images showing the spatial expression of OTX2 and HOXB4 of human ESCs induced with a lower concentration (1

ng/ml) or a higher concentration (10 ng/ml) of BMP4. (C). Colorimetric maps showing the average fluorescent intensity of OTX2 and HOXB4 staining. The intensity of each pixel of the images was normalized to the maximum value for each image. $n > 15$. (D). Plots showing the quantitative average intensity of OTX2 and HOXB4 in relation to the distance to the center of the pattern. Scale bar, 100 μm.

Figure 4

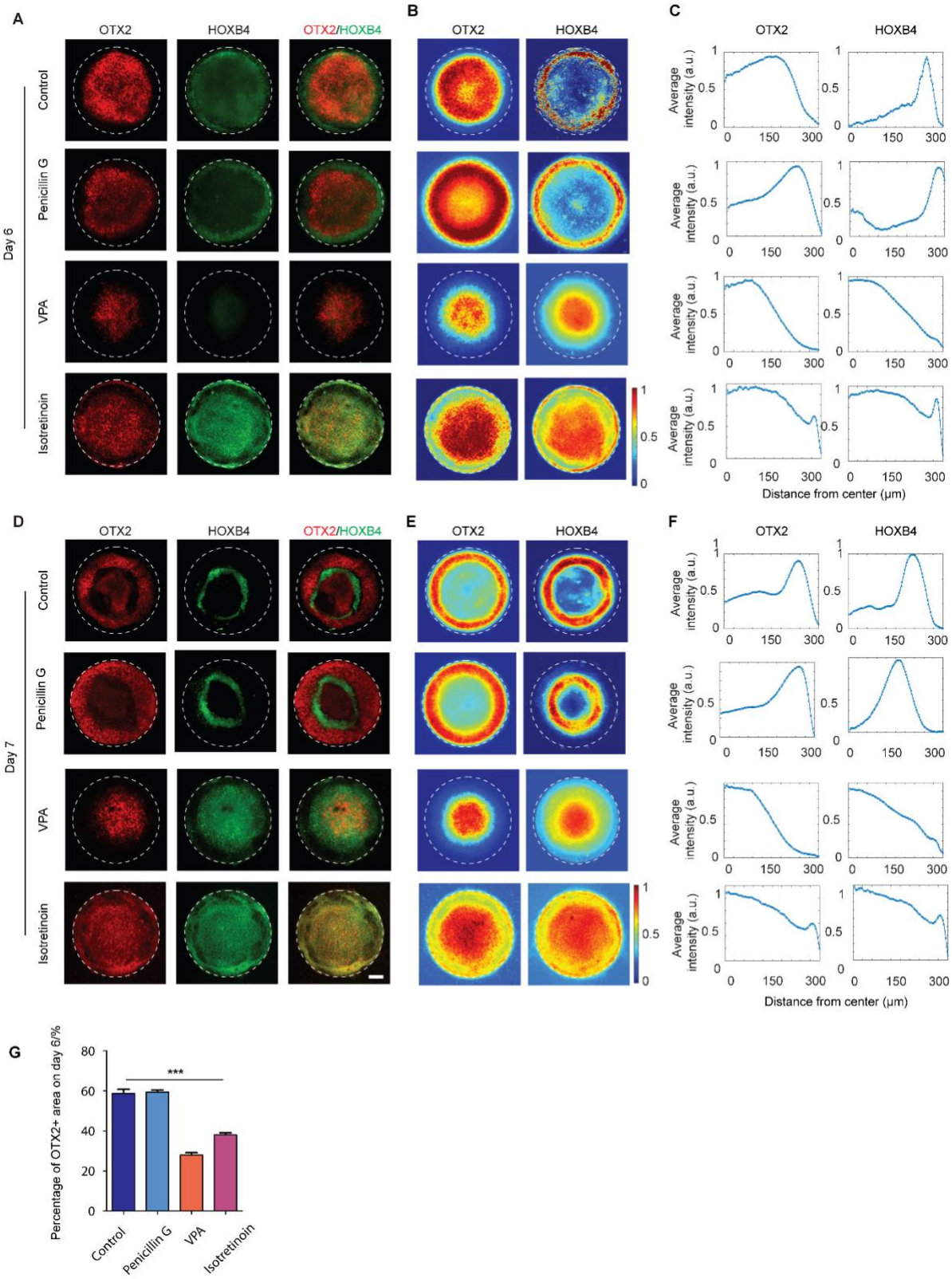
A
OTX2
HOXB4
OTX2/HOXB4
Day 6
Control
Penicillin G
VPA
Isotretinoin
B
OTX2
HOXB4
C
OTX2
HOXB4
Average intensity (a.u.)
Distance from center (μm)
D
OTX2
HOXB4
OTX2/HOXB4
Day 7
Control
Penicillin G
VPA
Isotretinoin
E
OTX2
HOXB4
F
OTX2
HOXB4
Average intensity (a.u.)
Distance from center (μm)
G
Percentage of OTX2+ area on day 6/%
***
Control
Penicillin G
VPA
Isotretinoin

Figure 4. The effects of medium dosages of penicillin G, valproic acid, and isotretinoin on anteroposterior patterning of OTX2 and HOXB4. (A). Representative immunostaining fluorescence images showing the spatial expression of OTX2 and HOXB4 in induced human ESCs treated with DMSO (control) and medium dosages of penicillin G, valproic acid, and isotretinoin on day 6. (B). Colorimetric maps showing the average fluorescent intensity of OTX2 and HOXB4 staining. The intensity of each pixel of the images was normalized to the maximum value for each image. $n > 15$. (C). Plots showing the quantitative average intensity in relation to the distance to the center of the pattern. (D). Representative immunostaining fluorescence images showing the spatial expression of OTX2 and HOXB4 in induced human ESCs treated with DMSO (control) and medium dosages of penicillin G, valproic acid, and isotretinoin on day 7. (E). Colorimetric maps showing the average fluorescent intensity of OTX2 and HOXB4 staining. The intensity of each pixel of the images was normalized to the maximum value for each image. $n > 15$. (F). Plots showing the quantitative average intensity in relation to the distance to the center of the pattern. (G). The percentage of area covered by OTX2+ midbrain in DMSO control, penicillin G, VPA, and isotretinoin treated groups. Scale bar, 100 μm. Data are represented as mean ± s.e.m. ***, $P < 0.001$.

REFERENCE

1 Salehi, H. *et al.* Differentiation of human ES cell-derived neural progenitors to neuronal cells with regional specific identity by co-culturing of notochord and somite. *Stem Cell Res* **8**, 120-133, doi:10.1016/j.scr.2011.08.008 (2012).

2 Harada, H., Sato, T. & Nakamura, H. Fgf8 signaling for development of the midbrain and hindbrain. *Dev Growth Differ* **58**, 437-445, doi:10.1111/dgd.12293 (2016).

3 Ishikawa, Y., Yamamoto, N., Yoshimoto, M. & Ito, H. The primary brain vesicles revisited: are the three primary vesicles (forebrain/midbrain/hindbrain) universal in vertebrates? *Brain Behav Evol* **79**, 75-83, doi:10.1159/000334842 (2012).

4 Gibbs, H. C., Chang-Gonzalez, A., Hwang, W., Yeh, A. T. & Lekven, A. C. Midbrain-Hindbrain Boundary Morphogenesis: At the Intersection of Wnt and Fgf Signaling. *Front Neuroanat* **11**, 64, doi:10.3389/fnana.2017.00064 (2017).

5 Lumsden, A. & Krumlauf, R. Patterning the vertebrate neuraxis. *Science* **274**, 1109-1115, doi:10.1126/science.274.5290.1109 (1996).

6 Kiecker, C. & Lumsden, A. The role of organizers in patterning the nervous system. *Annu Rev Neurosci* **35**, 347-367, doi:10.1146/annurev-neuro-062111-150543 (2012).

7 Kiecker, C. & Lumsden, A. Compartments and their boundaries in vertebrate brain development. *Nat Rev Neurosci* **6**, 553-564, doi:10.1038/nrn1702 (2005).

8 Londin, E. R., Niemiec, J. & Sirotkin, H. I. Chordin, FGF signaling, and mesodermal factors cooperate in zebrafish neural induction. *Dev Biol* **279**, 1-19, doi:10.1016/j.ydbio.2004.11.016 (2005).

9 Fouquet, B., Weinstein, B. M., Serluca, F. C. & Fishman, M. C. Vessel patterning in the embryo of the zebrafish: guidance by notochord. *Dev Biol* **183**, 37-48, doi:10.1006/dbio.1996.8495 (1997).

10 Wittler, L. & Kessel, M. The acquisition of neural fate in the chick. *Mech Dev* **121**, 1031-1042, doi:10.1016/j.mod.2004.05.004 (2004).

11 Wang, M., Ling, K. H., Tan, J. J. & Lu, C. B. Development and Differentiation of Midbrain Dopaminergic Neuron: From Bench to Bedside. *Cells* **9**, doi:10.3390/cells9061489 (2020).

12 Gerhart, J. in *Conceptual Change in Biology: Scientific and Philosophical Perspectives on Evolution and Development* (ed Alan C. Love) 175-197 (Springer Netherlands, 2015).

13 Koch, P., Opitz, T., Steinbeck, J. A., Ladewig, J. & Brustle, O. A rosette-type, self-renewing human ES cell-derived neural stem cell with potential for in vitro instruction and synaptic integration. *Proc Natl Acad Sci U S A* **106**, 3225-3230, doi:10.1073/pnas.0808387106 (2009).

14 Yan, Y. *et al.* Directed differentiation of dopaminergic neuronal subtypes from human embryonic stem cells. *Stem Cells* **23**, 781-790, doi:10.1634/stemcells.2004-0365 (2005).

15 Moris, N. *et al.* An in vitro model of early anteroposterior organization during human development. *Nature* **582**, 410-415, doi:10.1038/s41586-020-2383-9 (2020).

16 Meinhardt, A. *et al.* 3D Reconstitution of the Patterned Neural Tube from Embryonic Stem Cells. *Stem Cell Reports* **3**, 987-999, doi:10.1016/j.stemcr.2014.09.020 (2014).

17 Zheng, Y. *et al.* Dorsal-ventral patterned neural cyst from human pluripotent stem cells in a neurogenic niche. *Science Advances* **5**, eaax5933, doi:10.1126/sciadv.aax5933 (2019).

18 Demers, C. J. *et al.* Development-on-chip: in vitro neural tube patterning with a microfluidic device. *Development* **143**, 1884-1892, doi:10.1242/dev.126847 (2016).

19 Bagley, J. A., Reumann, D., Bian, S., Levi-Strauss, J. & Knoblich, J. A. Fused cerebral organoids model interactions between brain regions. *Nat Methods* **14**, 743-751, doi:10.1038/nmeth.4304 (2017).
20 Birey, F. *et al.* Assembly of functionally integrated human forebrain spheroids. *Nature* **545**, 54-59, doi:10.1038/nature22330 (2017).
21 Cederquist, G. Y. *et al.* Specification of positional identity in forebrain organoids. *Nat Biotechnol* **37**, 436-444, doi:10.1038/s41587-019-0085-3 (2019).
22 Kirkeby, A. *et al.* Generation of regionally specified neural progenitors and functional neurons from human embryonic stem cells under defined conditions. *Cell Rep* **1**, 703-714, doi:10.1016/j.celrep.2012.04.009 (2012).
23 Lippmann, E. S. *et al.* Deterministic HOX patterning in human pluripotent stem cell-derived neuroectoderm. *Stem Cell Reports* **4**, 632-644, doi:10.1016/j.stemcr.2015.02.018 (2015).
24 Hu, B. Y. & Zhang, S. C. Differentiation of spinal motor neurons from pluripotent human stem cells. *Nat Protoc* **4**, 1295-1304, doi:10.1038/nprot.2009.127 (2009).
25 Rifes, P. *et al.* Modeling neural tube development by differentiation of human embryonic stem cells in a microfluidic WNT gradient. *Nat Biotechnol* **38**, 1265-1273, doi:10.1038/s41587-020-0525-0 (2020).
26 Mica, Y., Lee, G., Chambers, S. M., Tomishima, M. J. & Studer, L. Modeling neural crest induction, melanocyte specification, and disease-related pigmentation defects in hESCs and patient-specific iPSCs. *Cell Rep* **3**, 1140-1152, doi:10.1016/j.celrep.2013.03.025 (2013).
27 Xie, T., Hawkins, J. & Sun, Y. in *Fibrosis: Methods and Protocols* (ed Laure Rittié) 235-244 (Springer New York, 2017).
28 Xue, X. *et al.* Mechanics-guided embryonic patterning of neuroectoderm tissue from human pluripotent stem cells. *Nature Materials* **17**, 633-641, doi:10.1038/s41563-018-0082-9 (2018).
29 Xie, T., Kang, J., Pak, C., Yuan, H. & Sun, Y. Temporal Modulations of NODAL, BMP, and WNT Signals Guide the Spatial Patterning in Self-Organized Human Ectoderm Tissues. *Matter*, doi:10.1016/j.matt.2020.04.012 (2020).
30 Brady, M. V. & Vaccarino, F. M. Role of SHH in Patterning Human Pluripotent Cells towards Ventral Forebrain Fates. *Cells* **10**, 914, doi:10.3390/cells10040914 (2021).
31 Steinberg, M. S. On the mechanism of tissue reconstruction by dissociated cells. I. Population kinetics, differential adhesiveness. and the absence of directed migration. *Proc Natl Acad Sci U S A* **48**, 1577-1582, doi:10.1073/pnas.48.9.1577 (1962).
32 Schötz, E. M. *et al.* Quantitative differences in tissue surface tension influence zebrafish germ layer positioning. *Hfsp j* **2**, 42-56, doi:10.2976/1.2834817 (2008).
33 Muncie, J. M. *et al.* Mechanical Tension Promotes Formation of Gastrulation-like Nodes and Patterns Mesoderm Specification in Human Embryonic Stem Cells. *Developmental Cell* **55**, 679-694.e611, doi:10.1016/j.devcel.2020.10.015 (2020).
34 Brown, N. A., Kao, J. & Fabro, S. Teratogenic Potential of Valproic Acid. *Lancet* **1**, 660-661 (1980).
35 Robert, E. & Guibaud, P. Maternal Valproic Acid and Congenital Neural-Tube Defects. *Lancet* **2**, 937-937, doi:DOI 10.1016/s0140-6736(82)90908-4 (1982).

36 Asgari, S. *et al.* Differentiation and Transplantation of Human Induced Pluripotent Stem Cell-derived Hepatocyte-like Cells. *Stem Cell Reviews and Reports* **9**, 493-504, doi:10.1007/s12015-011-9330-y (2013).
37 Abroms, L., Maibach, E., Lyon-Daniel, K. & Feldman, S. R. What is the best approach to reducing birth defects associated with isotretinoin? *Plos Med* **3**, 1978-1983, doi:ARTN e483

10.1371/journal.pmed.0030483 (2006).
38 Muhsen, M. *et al.* Folic acid supplementation rescues valproic acid-induced developmental neurotoxicity and behavioral alterations in zebrafish embryos. *Epilepsia*, doi:10.1111/epi.16915 (2021).
39 Hughes, A., Greene, N. D. E., Copp, A. J. & Galea, G. L. Valproic acid disrupts the biomechanics of late spinal neural tube closure in mouse embryos. *Mech Dev* **149**, 20-26, doi:10.1016/j.mod.2017.12.001 (2018).
40 Merlini, L., Fluss, J., Dhouib, A., Vargas, M. I. & Becker, M. Mid-hindbrain malformations due to drugs taken during pregnancy. *J Child Neurol* **29**, 538-544, doi:10.1177/0883073812474345 (2014).
41 Rizzo, R., Lammer, E. J., Parano, E., Pavone, L. & Argyle, J. C. Limb Reduction Defects in Humans Associated with Prenatal Isotretinoin Exposure. *Teratology* **44**, 599-604, doi:DOI 10.1002/tera.1420440602 (1991).
42 Landis, E. T. *et al.* Isotretinoin and oral contraceptive use in female acne patients varies by physician specialty: analysis of data from the National Ambulatory Medical Care Survey. *Journal of Dermatological Treatment* **23**, 272-277, doi:10.3109/09546634.2012.671908 (2012).
43 Suuberg, A. Psychiatric and Developmental Effects of Isotretinoin (Retinoid) Treatment for Acne Vulgaris. *Current Therapeutic Research* **90**, 27-31, doi:10.1016/j.curtheres.2019.01.008 (2019).
44 Xing, J., Toh, Y.-C., Xu, S. & Yu, H. A method for human teratogen detection by geometrically confined cell differentiation and migration. **5**, 10038, doi:10.1038/srep10038 (2015).
45 Sahni, G. *et al.* A Micropatterned Human-Specific Neuroepithelial Tissue for Modeling Gene and Drug-Induced Neurodevelopmental Defects. *Adv Sci (Weinh)* **8**, 2001100, doi:10.1002/advs.202001100 (2021).
46 Plaut, M. E., O'Connell, C. J., Pabico, R. C. & Davidson, D. Penicillin handling in normal and azotemic patients. *J Lab Clin Med* **74**, 12-18 (1969).
47 Wurst, W. & Bally-Cuif, L. Neural plate patterning: upstream and downstream of the isthmic organizer. *Nat Rev Neurosci* **2**, 99-108, doi:10.1038/35053516 (2001).
48 Martyn, I., Kanno, T. Y., Ruzo, A., Siggia, E. D. & Brivanlou, A. H. Self-organization of a human organizer by combined Wnt and Nodal signalling. *Nature* **558**, 132-135, doi:10.1038/s41586-018-0150-y (2018).
49 Chhabra, S., Liu, L., Goh, R., Kong, X. & Warmflash, A. Dissecting the dynamics of signaling events in the BMP, WNT, and NODAL cascade during self-organized fate patterning in human gastruloids. *PLoS Biol* **17**, e3000498, doi:10.1371/journal.pbio.3000498 (2019).
50 Arpino, C. *et al.* Teratogenic effects of antiepileptic drugs: Use of an international database on malformations and drug exposure (MADRE). *Epilepsia* **41**, 1436-1443, doi:DOI 10.1111/j.1528-1157.2000.tb00119.x (2000).

51 Alessandri, J. L. *et al.* Tibial Developmental Field Defect in Valproic Acid Embryopathy: Report on Three Cases. *Am J Med Genet A* **152a**, 2805-2809, doi:10.1002/ajmg.a.33633 (2010).
52 Christensen, J. *et al.* Prenatal Valproate Exposure and Risk of Autism Spectrum Disorders and Childhood Autism. *Jama-J Am Med Assoc* **309**, 1696-1703, doi:10.1001/jama.2013.2270 (2013).
53 Silvestrin, R. B. *et al.* Animal model of autism induced by prenatal exposure to valproate: Altered glutamate metabolism in the hippocampus. *Brain Res* **1495**, 52-60, doi:10.1016/j.brainres.2012.11.048 (2013).
54 Chanda, S. *et al.* Direct Reprogramming of Human Neurons Identifies MARCKSL1 as a Pathogenic Mediator of Valproic Acid-Induced Teratogenicity. *Cell Stem Cell* **25**, 103-+, doi:10.1016/j.stem.2019.04.021 (2019).
55 Cui, K. *et al.* Neurodevelopmental impairment induced by prenatal valproic acid exposure shown with the human cortical organoid-on-a-chip model. *Microsyst Nanoeng* **6**, 49, doi:10.1038/s41378-020-0165-z (2020).
56 Makori, N., Peterson, P. E. & Hendrickx, A. G. 13-cis-retinoic acid causes patterning defects in the early embryonic rostral hindbrain and abnormal development of the cerebellum in the macaque. *Teratology* **63**, 65-76 (2001).
57 Holson, R. R. *et al.* Gestational retinoic acid exposure: A sensitive period for effects on neonatal mortality and cerebellar development. *Neurotoxicology and Teratology* **19**, 335-346, doi:10.1016/s0892-0362(97)00039-1 (1997).
58 McCaffery, P. J., Adams, J., Maden, M. & Rosa-Molinar, E. Too much of a good thing: retinoic acid as an endogenous regulator of neural differentiation and exogenous teratogen. *European Journal of Neuroscience* **18**, 457-472, doi:10.1046/j.1460-9568.2003.02765.x (2003).